Curvature of interatomic surfaces. I. Fundamentals

A. Martín Pendás[a] and V. Luaña
Departamento de Química Física y Analítica, Facultad de Química, Universidad de Oviedo, E-33006-Oviedo, Spain

(Received 15 May 2003; accepted 21 July 2003)

Some basic aspects regarding the geometry of the interatomic surfaces of the theory of atoms in molecules are considered. After showing that the global Gauss–Bonnet theorem poses severe difficulties on the calculation of the total Gaussian curvatures of unbounded interatomic surfaces, we propose the use of the local value of the Gaussian curvature at the bond critical point as a better suited indicator of the geometry of the surfaces. To that end, we report analytical expressions for the curvatures of gradient lines and interatomic surfaces at critical points. © *2003 American Institute of Physics.* [DOI: 10.1063/1.1607963]

I. INTRODUCTION

The theory of atoms in molecules (AIM) developed by R. L. Bader and coworkers[1] has shown how an exhaustive partition of the physical space into disjoint regions may be found such that (i) the quantum mechanics of a subregion is well defined and (ii) the regions can be faithfully identified with the atoms of chemistry. This partition is induced by the topology of the electron density scalar field (ρ), and the atoms are identified with the attraction basins of the gradient vector field of the charge density. The topological elements of the $\nabla\rho$ field are the carriers of a wealth of chemically relevant information, and the critical points ($\nabla\rho=\mathbf{0}$), for instance, are the generators of the molecular graph.[2] The theory has been extremely successful in recovering chemical concepts from both experimental[3] and theoretical[1] densities, and it is now well developed in both the molecular[4] and condensed matter[5] realms.

The three-dimensional (3D) attraction basin of a given maximum of ρ—i.e., the geometric locus of all points with gradient (flux) lines of $\nabla\rho$ ending up at the selected maximum—is separated from the rest of the space by a 2D separatrix called the interatomic surface (IAS). It corresponds to the union of all the attraction basins of the first-order saddles of the ρ field [bond critical points (bcp's)] to which the maximum is connected (bonded). The direct or indirect determination of IASs is a key step in the computation of atomic properties by integrating appropriate operator densities over the atomic basins.[6] The values of several important observable densities over the IASs are also crucial in order to develop the quantum theory of stress within the AIM formalism.[7] It is also possible to transform several 3D integrations over atomic basins into surface integrals over IASs.[8] Much work has therefore been devoted to the efficient computational construction of IASs. This has turned out to be a difficult enterprise, for IASs lack a unique local description, being only globally defined. Very often, the separatrices are referred to as zero-flux surfaces, since they locally fulfill $\nabla\rho(\boldsymbol{r})\cdot\boldsymbol{n}(\boldsymbol{r})=\mathbf{0}$, where $\boldsymbol{n}$ is a normal vector to the surface. However, this is a necessary but not sufficient condition for a separatrix. In fact, one may choose any continuous piece of a 1D curve $\boldsymbol{r}(t)$, $t\in[0,1]$, that is not itself a gradient line and integrate the gradient field of ρ at each of its points. We will obtain a one-parameter family of gradient lines, $\boldsymbol{g}_t(s)$, such that $d\boldsymbol{g}_t(s)/ds=\nabla\rho(\boldsymbol{g}_t(s))$ and $\boldsymbol{g}_t(0)=\boldsymbol{r}(t)$. This family is a 2D zero-local-flux surface, but not a separatrix.

The zero-flux condition could, in principle, be used to design efficient algorithms to locate IASs. However, the previous concern makes the construction of good algorithms a complex task. Several numerical methods to locate and integrate operator densities over IASs have been proposed. One of the most robust, though very inefficient, is a bipartition technique that exploits the fact that gradient lines started at one or the other side of the surface end up at different maxima. Much better alternatives include a variational determination of the surfaces proposed by Cioslowski and Stefanov,[9] which was later extended to obtain the response of the IASs to external perturbations,[10] and the various works by Popelier, who has examined analytical expansions and several numerical fitting procedures[11] to treat the problem.

A different issue is posed not by the calculation of IASs as tools to compute atomic properties, but by the geometry of the surfaces itself. Their shape and structure have raised interest as generators of images of atomic basins, and several visualization techniques have been devised, mainly by Popelier in molecular systems[12] and by ourselves in condensed phases.[5] The *a posteriori* examination of those shapes shows that the geometry of the IASs is characteristic of the type of bond under examination and clearly sensitive to the overall environment of that bond. In fact, the constancy of 2D projections of IASs across different molecules sharing a specific bond was one of the historical origins of the AIM theory. The increasing availability of accurate images of IASs has revealed their complex shapes.[13] Nevertheless and though acute spikes, winglike protrusions, and many other exotic features are common,[14] their curvature near bcp's has been shown to be intimately related to the charge transfer associated with the bond. For instance, in our works on largely ionic compounds,[14] we have invariably found that convex surfaces signal cations and concave surface anions. The

[a]Electronic mail: angel@fluor.quimica.uniovi.es

study of the geometry of the separatrices of $\nabla\rho$ may then lead to local indices related to integral properties that are, otherwise, difficult to obtain.

Actually, the differential geometry of IASs has been previously explored in a 1996 paper by Popelier.[15] The paper focused on the total or integral Gauss curvature of IASs, which was constructed by integrating the local Gaussian curvature (K) of a numerically fitted IAS, and disclosed how this scalar could be successfully related to polarizability, electronegativity, and chemical environment differences between the bonded atoms that generate a surface. However useful this total curvature concept may appear, it is still an integrated magnitude, and a rather large computational effort is needed to obtain it. Moreover, the global Gauss–Bonnett theorem poses several concerns on the computational accessibility of the total Gaussian curvatures of IASs.

The aim of this work is twofold. On the one hand, we will show that it is the value of K near bond critical points, and not the total curvature, which is to be pursued. As we will see, this is due to the extreme sensitivity of the total curvature to computational details, not only as the construction of the surfaces is regarded, but also as the quantum chemical model used to obtain the electron density is concerned. As a result and though the total curvature of an IAS is a well-defined magnitude, it is a basically inaccessible one, particularly when open surfaces are considered in isolated molecules. On the other hand, since IASs are fairly smooth near bcp's, K in their surroundings is well represented by its value at the bcp, K_{bcp}. We will show that it is possible to obtain analytical expressions for the principal curvatures of separatrices at critical points that only involve second and third derivatives of the charge density. K_{bcp} may in this way be obtained together with the electron density at almost no extra computational cost.

The work is structured as follows. Paper I will be devoted to the basic aspects of the global and local geometry of IASs. A number of necessary concepts from the differential geometry of bidimensional manifolds will also be presented, and a couple of actual examples will exemplify the discussion. In Paper II, we will use the local curvatures at bond critical points derived in Paper I to rationalize the origin of the curvatures of IASs. A hierarchy of approximate models will be used to throw light on this problem, and a number of simple molecules will be studied in detail as a first step towards the systematization of the actual curvatures found in molecular systems.

The rest of Paper I contains the following material. In Sec. II we introduce the basic notions of differential geometry that will be needed in the rest of the paper. These are, in fact, a set of definitions that complement those given in Popelier's paper.[15] This section may be skipped by any reader familiar with differential geometry. Section III is devoted to examine the global or intrinsic geometry of IASs in the light of the Gauss–Bonnet theorem. Both open and closed surfaces will be examined, and several questions concerning the computation of total curvatures will be presented. We will then turn in Sec. IV to consider how to obtain analytical formulas for the curvatures of gradient lines and IASs at critical points. A brief summary of these results will conclude the paper.

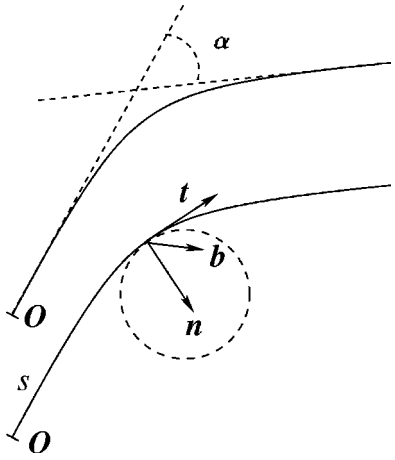

FIG. 1. Upper diagram: definition of the exterior angle change between the tangents at two points of a curve. Lower diagram: the Frenet frame of a curve parametrized by its arclength. κ^{-1}, the radius of curvature, coincides with the radius of a circumference with the same curvature as that of the curve.

II. NOTIONS ON THE DIFFERENTIAL GEOMETRY OF CURVES AND SURFACES

In this section we are going to present a small, biased set of definitions and results on the differential geometry of curves and surfaces in 3D physical space. We feel this is necessary in order to reach a general audience that may not be fully familiar with these notions. A standard, easily accessible reference for physicists and chemists is the text by do Carmo,[16] and a recent review regarding these topics in a physical context is that by Kamien.[17] We will also present a couple of more specific results that will be needed in the following.

Gradient lines of a 3D vector field are curves in space. A parametrized differentiable curve is a smooth function $\boldsymbol{r}(t):I\rightarrow\mathbb{R}^3$, where $I=(a,b)$ is a given interval of $\mathbb{R}$. A distinguished parametrization is generated by the arclength $s(t)=\int_a^t|\boldsymbol{r}'|dt$. Let $\boldsymbol{r}(s)$ be parametrized by its arclength. The unit vector $\boldsymbol{t}=\boldsymbol{r}'$ is called the unit tangent of the curve. Points where the unit tangent vanishes are critical or singular points, and a curve without singular points is named regular. The module of the vector $\boldsymbol{r}''$ is the curvature scalar κ and the unit vector $\boldsymbol{n}=\kappa^{-1}\boldsymbol{t}'$, the principal normal. The vector $\boldsymbol{b}=\boldsymbol{t}\times\boldsymbol{n}$ is the binormal, the $\boldsymbol{t}$-$\boldsymbol{n}$ plane the osculator plane, and the $\boldsymbol{t}$, $\boldsymbol{n}$, $\boldsymbol{b}$ basis the Frenet reference frame of the curve at a given point (see Fig. 1). The scalar τ defined by $\boldsymbol{b}'=-\tau\boldsymbol{n}'$ is called the torsion, and the fundamental theorem of the local theory of curves states that given the functions $\kappa(s)>0$ and $\tau(s)$, there is only one curve, defined up to a given rigid motion, whose curvature and torsion are given by those functions. As a global result, it is easy to show that $\alpha=\int_a^b\kappa ds$ is the exterior angle change between the tangents of the curve at points $\boldsymbol{r}(a)$ and $\boldsymbol{r}(b)$. The reader may check that if a curve is only piecewise regular, the previous expression is still valid if we assume that an additive *impulse* curvature, or

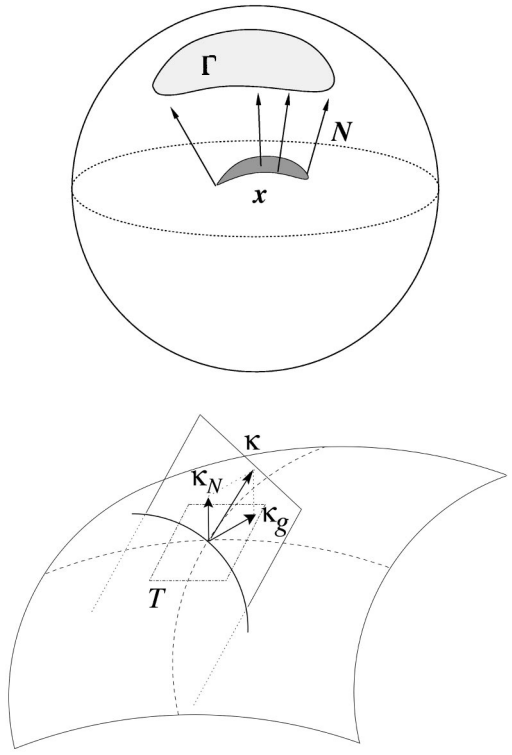

FIG. 2. Upper diagram: the Gauss map. The unit normal field $\boldsymbol{n}$ of a surface patch $\boldsymbol{x}$ maps the surface onto the unit sphere and associates a particular area Γ to the surface. Lower diagram: decomposition of the curvature vector $\boldsymbol{r}''(s)$ of an arclength parametrized curve embedded onto a surface into its tangential and normal components. Their moduli are the geodesic and normal curvatures of the curve, respectively.

angle defect, is present at each angular point, $\boldsymbol{r}_{\text{ang}}$, and equal to the exterior angle change between the left and right tangents of the curve at $\boldsymbol{r}_{\text{ang}}$.

A parametric surface patch is a smooth function $\boldsymbol{x}(u_1,u_2):U\rightarrow\mathbb{R}^3$, where $U\subset\mathbb{R}^2$ is an open set and the Jacobian of $\boldsymbol{x}$ is nonsingular. The tangent space of $\boldsymbol{x}$ at $p\subset U$, $T_p\boldsymbol{x}$, is the 2D subspace generated by the vectors $\boldsymbol{x}_1(p)$ and $\boldsymbol{x}_2(p)$. The tangent plane is the affine space $\boldsymbol{x}(p)+T_p\boldsymbol{x}$, and the unit vector field $\boldsymbol{N}=(\boldsymbol{x}_1\times\boldsymbol{x}_2)/|\boldsymbol{x}_1\times\boldsymbol{x}_2|$ is called the unit normal. If it is possible to construct a differentiable unit normal field over the whole surface, we say the surface is orientable. The map $\boldsymbol{N}:U\rightarrow\mathbb{S}^2$ of the normal field onto the unit sphere is called the Gauss map of the surface and is sketched in Fig. 2. Minus the tangential directional derivative of the unit normal is a symmetric bilinear form, the Weingarten tensor or second fundamental form, which measures the change of the tangent plane when moving onto the surface. Its components in the u coordinates are $\kappa_{ij}=\boldsymbol{x}_{ij}\cdot\boldsymbol{N}$. If $\boldsymbol{t}$ is the unit tangent to an arclength parametrized curve $\boldsymbol{r}(s)$ on the surface, $\kappa(\boldsymbol{t},\boldsymbol{t})$ equals $\boldsymbol{r}''(s)\cdot\boldsymbol{N}$, the normal curvature of the curve, κ_N. The projection of $\boldsymbol{r}''(s)$ onto the tangent plane is called the geodesic curvature κ_g. These relations are also visualized in Fig. 2. The elevation of a surface above its tangent plane at $\boldsymbol{x}(u)$ is given, up to second-order terms, by $h(v)=1/2\Sigma_{ij}\kappa_{ij}(v-u)_i(v-u)_j$. This is the osculating paraboloid that we will use in the following. The minimum, κ_1, and maximum, κ_2, normal curvatures are the principal

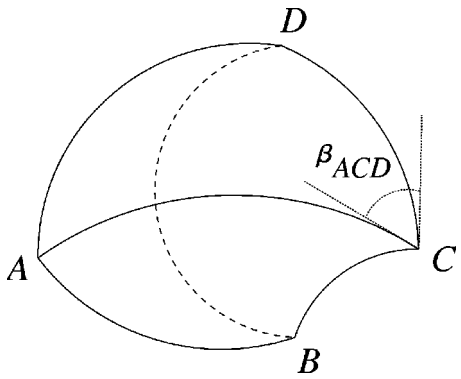

FIG. 3. A surface homeomorphic to a tetrahedron. The interior angle at the C vertex coming from the ACD surface; β_{ACD} is explicitly shown. The tetrahedron may be closed or open. If the face BCD is lacking, for instance, the BCD curve is the boundary, and the C vertex is a boundary vertex.

curvatures of the surface at a point and their orthogonal tangent directions its principal directions. The two invariants of the second form are the mean curvature $H=1/2(\kappa_1+\kappa_2)$ and the Gauss curvature $K=\kappa_1\kappa_2$.

Of utmost importance is the Gauss–Bonnett (GB) theorem, one of the deepest results in the differential geometry of surfaces. In its local version, it states that for a simply connected oriented surface patch S with a regular curve $\boldsymbol{r}(s)$ as its boundary, $\partial S=\boldsymbol{r}$, $\int_S Kd\sigma+\int_{\boldsymbol{r}}\kappa_g ds=2\pi$. The first term may be identified with the area Γ of Fig. 2. If the boundary is only piecewise regular, there are impulse curvatures α_i at the ith junction, and the theorem generalizes to $\int_S Kd\sigma+\int_{\boldsymbol{r}}\kappa_g ds+\Sigma_i\alpha_i=2\pi$. By triangulating a general surface one gets the global version of the Gauss–Bonnet formula, which states that if $\boldsymbol{r}$ is a piecewise regular curve bounding a region S of an oriented surface, then $\int_S Kd\sigma+\int_{\boldsymbol{r}}\kappa_g ds+\Sigma_i\alpha_i=2\pi\chi$, where χ is the Euler–Poincaré characteristic of the surface, an invariant that may be obtained by the Euler formula $F-E+V=\chi$, where F, E, and V are the number of faces, edges, and vertices of the triangulation. For a compact regular surface homomorphic to a sphere, $\chi=2$, $C=\int Kd\sigma=4\pi$, and the total, or integral, curvature is invariant. This result may be understood very clearly from the area Γ enclosed by the Gauss map of Fig. 2 if the surface closes.

It is not very usual to find adequate generalizations of the GB theorem for surfaces with impulse curvature at points not belonging to the boundary—for instance, polyhedra. The total curvature C of a *genus*-0 polyhedron like a cube is obviously 4π. If we construct its Gauss map, we will observe that all the curvature is stored at the vertices, each one contributing $\pi/2$ to the Γ area in the map. If the edges were not geodesics or the faces displayed Gaussian curvatures different from zero, they would also contribute to C. It is possible to join all these ideas into a rather general expression.[18] Since our aim are IASs, we are only going to consider surfaces which are homeomorphic to open or closed polyhedra—that is, surfaces with well-defined faces, edges, and vertices that will be allowed to display nonsmooth behavior only at edges and vertices. An example is shown in Fig. 3.

In order to keep the expressions simple, we will exclude cone points, though they may indeed be treated quite simi-

larly. Each of the faces of our surfaces is homeomorphic to a polygon. Let us call the interior angles at each of its vertices $\beta_i = \pi - \alpha_i$, where the α's are the exterior angles previously defined. Let us also construct at each polyhedral vertex V the sum of all the interior angles coming from the faces generating the vertex, $\Sigma_{i\in V}\beta_i$, and define the vertex impulse curvature I^V in the following way: (i) If the vertex is a boundary vertex (see Fig. 3), then $I^V = \pi - \Sigma_{i\in V}\beta_i$; (ii) otherwise, $I^V = 2\pi - \Sigma_{i\in V}\beta_i$. In a similar way, impulse curvatures are associated to each edge E by adding the (orientation preserving) integrated geodesic curvatures for the faces F_i that share it: (i) If the edge is at the boundary, $I^E = \int_{\mathbf{r}} \kappa_g^F ds$; (ii) if not, $I^E = \int_{\mathbf{r}} (\kappa_g^{F_1} + \kappa_g^{F_2}) ds$. Finally, each face (a regular patch) will display an integrated Gaussian curvature $C^F = \int_F K^F d\sigma$. With these definitions, the global GB theorem acquires the following form:

$$C = \sum_F C^F + \sum_V I^V + \sum_E I^E = 2\pi\chi. \tag{1}$$

It is important to notice that C^F has been the basic object of investigation in the previous work by Popelier[15] and that the most relevant information that the curvature of IASs may contain will be concentrated near charge accumulation regions, usually far from the boundaries of the IASs. In other words, C^F should be the most chemically relevant part of Eq. (1), though we will argue that it is the local curvature, and not the global one, which should be pursued.

III. GLOBAL GEOMETRY OF INTERATOMIC SURFACES

As previously noticed, the attraction or repulsion basins[5] of the different kinds of critical points of ρ can be related to the structural elements of chemistry. The repulsion line of a bcp, or bond path (i.e., the set of gradient lines that start at the critical point), signals the atoms bonded, while the attraction surface, the IAS, determines the 2D region that separates them. Different IASs may intersect. When they do, the intersection line is usually the attraction basin of a ring critical point, and two or more of these lines may also intersect at a cage critical point. In this manner, IASs, ring lines, and cage points can be associated with faces, edges, and vertices, respectively, of a polyhedral structure that encloses a local maximum of the electron density.[5] More exotic critical point connectivities[19] do occur in odd situations, are handled in equivalent ways, and will not be considered. From the geometric point of view, edges and vertices are the nonregular domains of atomic surfaces, and the sources of curvature are to be found in the different critical points: bcp's are the source of the Gaussian curvature of the regular domains of the IASs and ring and cage points the origin of impulse curvatures or angle defects.

A. General results

In general IASs may then be (i) completely unbounded, like in diatomics; (ii) partially bounded, like the IASs in a symmetrical triangular triatomic; (iii) completely bounded, like in infinite solids. Figure 4 sketches these three possibilities.

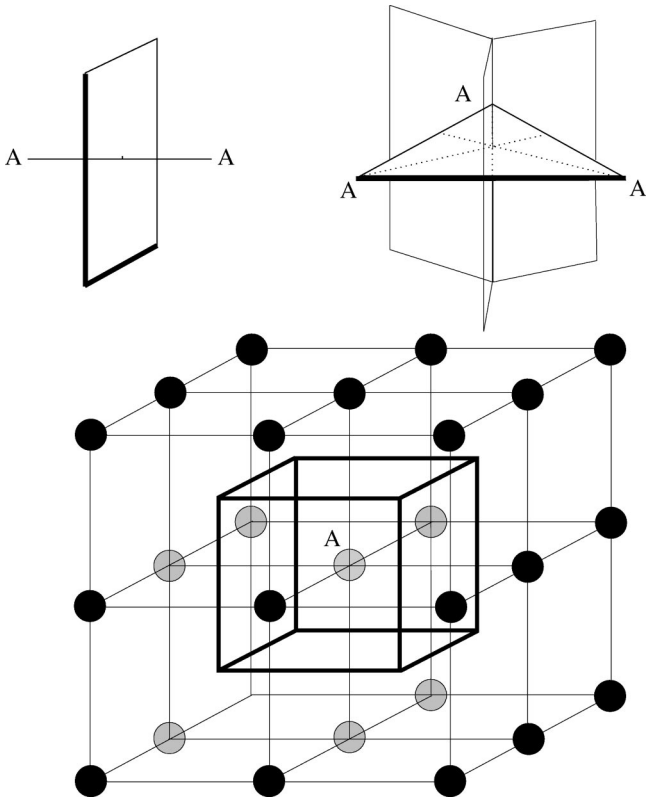

FIG. 4. The three basic kinds of IASs. (a) Unbound surface in a A_2 homonuclear diatomic. The IAS is an infinite plane that bisects both nuclei. (b) Partially bounded surfaces in an equilateral triangle A_3 triatomic. Each of the three equivalent surfaces is an infinite semiplane, its boundary being the attraction basin of the ring point situated at the center of the triangle. (c) Bounded surfaces in a simple cubic monoatomic A lattice. The six equivalent IASs of the central atom are planar squares with sides equal to the lattice parameter. Each IAS is bounded by for ring lines that intersect themselves at cage points at the corners of a regular cube.

Let us start considering in detail unbounded IASs in diatomic systems. Their revolution symmetry makes them particularly suited to analytical analysis without losing any generality. If we choose the internuclear axis as the z axis of a Cartesian frame centered at the bcp, the most general IAS is described as a revolution surface produced by a a $z = f(r)$ generating function, r being the distance to the revolution axis, with $f(0) = 0$, and $f'(0) = 0$. The Gaussian curvature of such a surface at any point (r, ϕ) may be easily obtained:

$$K(r) = \frac{f'(r) f''(r)}{r[1 + f'^2(r)]^2} \tag{2}$$

and integrated over the surface from $r = 0$ to $r = R$,

$$C^F = \int_0^{2\pi} d\phi \int_0^R dr K(r,\phi) = 2\pi\left(1 - \frac{1}{\sqrt{1 + f'^2(R)}}\right). \tag{3}$$

If we take the $R = \infty$ limit, this expression means that the integral Gaussian curvature of the unbounded revolution surface varies from 0 to 2π and does only depend on the slope of its tangent plane at infinity.

No revolution surface may have negative integral curvature. Actually, the GB theorem may be applied if we consider

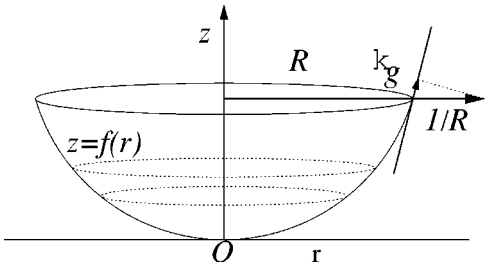

FIG. 5. A section of an otherwise infinite revolution surface cut by a plane orthogonal to the revolution axis. The geodesic curvature of the circular boundary is obtained by projecting its curvature $1/R$ onto the tangent plane.

a bounded patch of the surface as that shown in Fig. 5 and notice that the geodesic curvature of the closed boundary at a given point is

$$\kappa_g(R)=\frac{1}{R\sqrt{1+f'^2(R)}}. \tag{4}$$

Integrating over the circular boundary and adding the result to Eq. (3), we obtain that the C value 2π is that of an open regular surface in $\mathbb{R}^3$, independent of R, and that the integral geodesic curvature is generally nonvanishing at infinity.

Even if we consider just the total Gaussian curvature C^F, we see that its value is actually fixed by the slope of gradient lines at infinity with respect to the tangent plane at the bcp. As we will see, the computational inaccessibility of those slopes precludes the calculation of C^F in these cases. In partially bounded surfaces similar arguments apply to those regions of the IAS that escape to infinity.

Completely bounded surfaces are characteristic of inner atoms in large globular molecules or in infinite systems. In these cases, the atomic surfaces are homeomorphic to closed, convex polyhedra. As an example, Fig. 6 shows the atomic surface of the Li^+ cation in the rocksalt phase of the LiI crystal at its equilibrium geometry, as calculated with our *aim*PI method.[20] The cation displays six equivalent Li^+-I^- bonds, and the previously commented map onto a cube is evident. By recalling the Gauss map, it is clear that the whole atomic surface is a *genus*-0 surface with $C=4\pi$. Since there are impulse contributions from edges and vertices, each C^F is smaller than $4\pi/6$ and may be computed by a number of numerical methods, as previously shown. Notice, however, that the extension of any of these IASs is of the order of atomic spacings and that this implies that the curvature of any face is rather well represented by its value at the bcp. This fact, together with the difficulties for obtaining C^F in unbounded cases, leads us to propose the use of the local K values at bcp's, and not of the C^F integrals, as an standardized measure of the curvature of IASs.

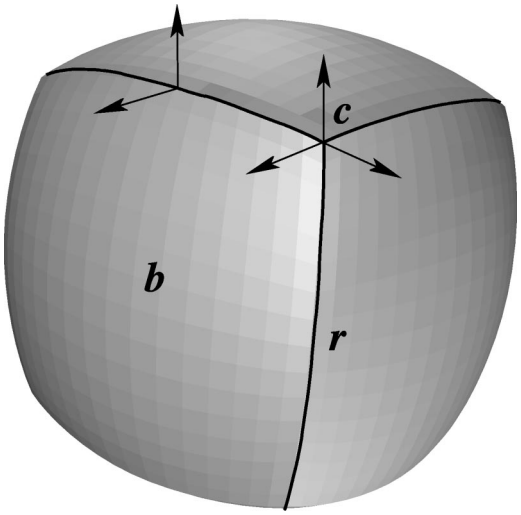

FIG. 6. Atomic surface of the Li^+ cation in LiI. The cation is at the center of the cube. The surface displays six equivalent convex IASs. Each face is the attraction basin of the a cation–anion bcp (b). The edges are the attraction basins of the 12 ring points (r) placed at their midpoints, and the vertices are 8 cage points (c). Unit normals at several points are displayed to show how impulse curvatures arise from both edges and vertices.

We turn now to consider the problem posed by unbounded surfaces in more detail.

B. Inaccessibility of the total Gaussian curvature in unbounded IASs

We have seen that in a diatomic IAS, C^F is controlled by the tangent plane slope at infinity. In this subsection we are going to show that this value, though well defined in principle, is not computationally accessible, for it is extremely sensitive to, actually determined by, the basis sets employed in the calculation. Our arguments are rather simple in the cylindrically symmetric surfaces of diatomics, but are of general validity in more complex situations, as we will show.

The question we want to address is the form of the asymptotic solutions of the dynamical system

$$\dot{\boldsymbol{r}}=\boldsymbol{\nabla}\rho(\boldsymbol{r}),\quad \lim_{t\to-\infty}\boldsymbol{r}=\boldsymbol{r}_{\mathrm{bcp}}, \tag{5}$$

where $\dot{\boldsymbol{r}}=d\boldsymbol{r}/dt$ is the derivative of the position vector with respect to a given t curve parametrization, at the $t\to\infty$ limit—that is, at infinite distance from a finite molecule. Much is not known about the asymptotic form of the electron density,[21] except that it decreases exponentially, $\rho\sim e^{-2\epsilon r}$, where ϵ is the first ionization potential and r is a distance to a fixed point in the molecule. All reasonable calculational procedures use basis sets, either exponential (almost exclusively in atoms or diatomics) or Gaussian, and it is almost always true that the most diffuse occupied primitive is of s type.

Let us first suppose that the diffuse primitive is centered at just one nucleus A. Then $\rho\sim e^{-\zeta r_A}$ (or $e^{-\zeta r_A^2}$) and

$$\frac{\rho_z}{\rho_x}\sim\frac{z}{x},\qquad \frac{\rho_z}{\rho_y}\sim\frac{z}{y},\qquad \frac{\rho_y}{\rho_x}\sim\frac{y}{x}, \tag{6}$$

where $\rho_\alpha=\partial\rho/\partial x_\alpha$. At sufficiently large distances from the molecule, then, the gradient field seems spherical, and all the flux lines are asymptotically straight lines pointing towards a sink located at the A nucleus. Reversely, a system of differ-

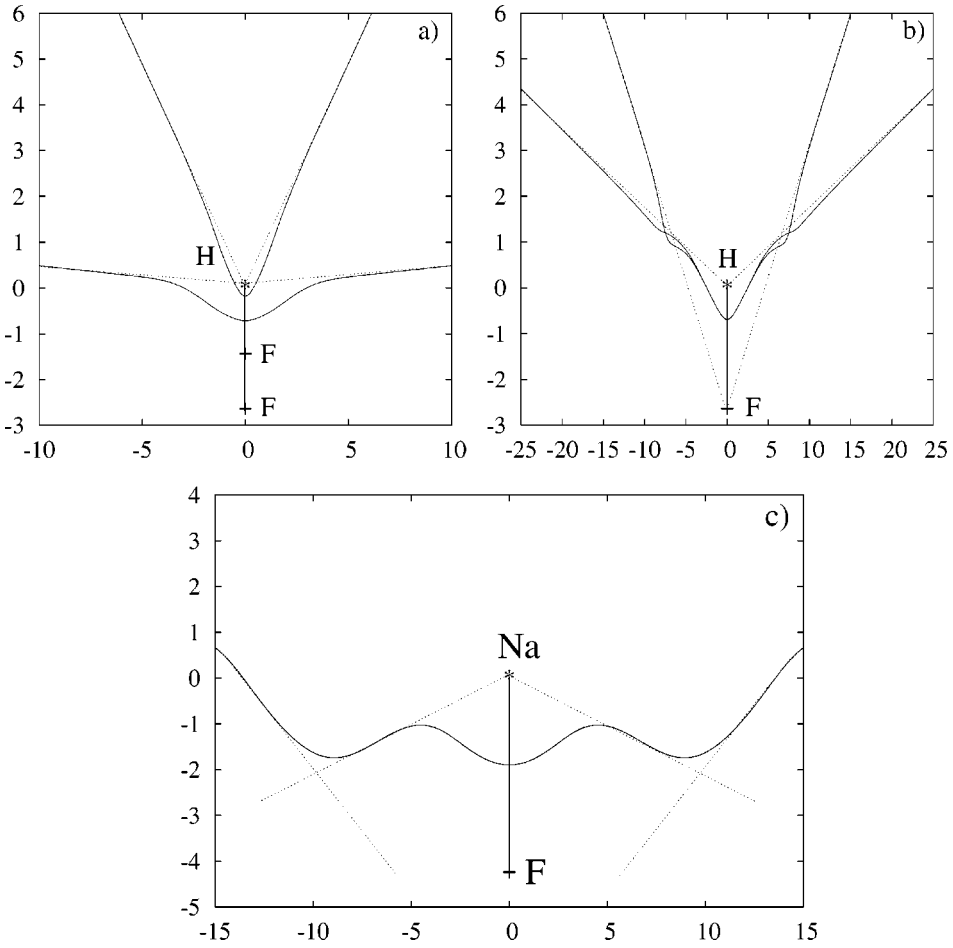

FIG. 7. Large distance behavior of IASs in diatomics. (a) Section of the HF/6-311G(p,d) IASs (solid line) of the HF molecule at internuclear distances $R=1.4$ and $R=2.6$ bohr. The H atom is placed at the origin, and all distances are measured in bohr. It is clearly seen that the asymptotic gradient lines (dotted lines) converge onto the hydrogen atom, which is the one who displays the most diffuse Gaussian, an s function with $\zeta=0.102\,741\,0$ bohr^{-2}. (b) HF/TZV($p,3d1f$) IASs of the same molecule at $R=2.6$ bohr with and without a diffuse s primitive with $\zeta=0.05$ bohr^{-2} centered at the fluorine nucleus. (c) HF/TZV IAS of NaF at $R=4.2$ bohr. Different spheres of influence are notorious.

ential equations satisfying Eq. (6) integrates to an spherically symmetric solution. If we follow one of these gradient lines starting from a point far away from the molecular center, the line will initially follow a straight trajectory directed towards the A nucleus. Eventually, it will notice the rest of the nuclei, its trajectory will curve, and it will finally end up at a given nucleus or critical point of the ρ field. Adding a more diffuse function to another nucleus—say, the B nucleus—will force all asymptotic lines to switch towards it without modifying their behavior near the molecule.

In a diatomic, knowledge of a single gradient line ending at the bcp determines the cylindrically symmetric IAS and, therefore, the slope of the asymptotic tangent plane with respect to the osculating plane at the bcp [$f'(\infty)$ in Eq. (3)]. Since the curvature of the IAS near the bcp is characteristic of the type of bond, the slope at infinity will depend on which nucleus bears the most diffuse primitive. This is a computational parameter that can be changed at will, so C^F is limited by our ability to describe electron densities at large distances from the molecular frame. This difficulty had already been put forward by Popelier,[15] who noticed that it is not reasonable to extend surface integrations to long distances. Here we show that C^F is determined by values at infinity, this fact precluding its use as an indicator of the geometry of IASs.

These ideas can immediately be contrasted in numerical experiments, though some care has to be taken when integrating the gradient vector field at large distances, for the simplest numerical procedures become highly unstable in such situations. We have used the robust an efficient VODE differential equations solver[22] as implemented in our molecular topology analyzer PROMOLDEN. The precision of the electronic structure calculations is not relevant in our discussion, and we only present results from small GAMESS (Ref. 23) Hartree–Fock calculations in a couple of test diatomics HF and NaF.

Figure 7(a) shows the 6-311G(p,d) IASs of HF at two internuclear distances $R=1.4$ and $R=2.6$ bohr projected onto a plane containing the internuclear axis. It is obvious that, with independence of the distance R, the center of forces of the gradient lines at infinity is the H atom, which bears the most diffuse Gaussian. Actually, a linear fit of the outer segments of both gradient lines gives straight lines with ordinates at the origin smaller than 10^{-6} bohr and correlation coefficients equal to 1 within 10^{-9}. The slopes of those fits give $f'(\infty)$ in Eq. (3) and are equal to 0.9789 and 0.048 61 for $R=1.4$ and 2.6 bohr, respectively. These are tantamount to their respective total C^F's, equal to 1.793 and 7.411×10^{-3}.

Figure 7(b) displays the change experimented by the IAS at constant geometry ($R=2.6$ bohr) introduced by just adding a diffuse s primitive to the fluorine basis set. The long-distance behavior, forced by the diffuse primitives as our algebraic arguments have shown, induces a complete reshaping of the surfaces. Notice how the region of chemical interest, near the bcp, is indeed extremely transferable, though the

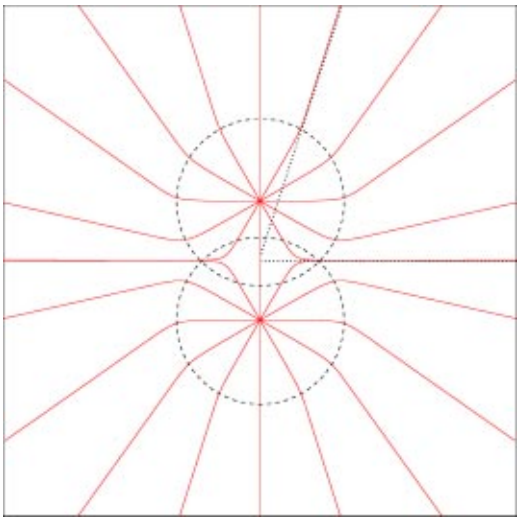

FIG. 8. $\nabla\rho$ field for a H_2 molecule with $R=1.4$ bohr in a plane containing the internuclear axis. The basis set of each atom consists of two $1s$ primitives with $\zeta_1=7.0$ and $\zeta_2=0.01$ a.u. See the text for details.

total C^F's change from 0.8282 to 0.091 05. It is tempting to integrate the Gaussian curvature only over a *chemically relevant* region. However, the size and shape of this zone are fairly arbitrary. Many authors use the $\rho=0.001$ a.u. envelope as its limit, but this definition can only be applied to unbounded surfaces. In bounded IASs the density is usually greater than that value at the boundary, making the construction of equivalent C^F's for bounded and unbounded surfaces impossible.

The behavior just shown may well be more colorful in many situations. Figure 7(c) shows how different regions of space may be dominated by a primitive or small collection of primitives of the basis set. When this occurs, the IAS develops rather linear regions pointing towards the relevant center that change direction when another primitive centered on another nucleus becomes dominant.

When more than one nucleus bears the same most diffuse primitive, the arguments flow in a similar way. For example, let us consider a homodiatomic with nuclei a,b centered at $(0,0,\pm\delta)$, respectively, and place diffuse $\phi_s\sim e^{-\zeta r}$ primitives centered on each nucleus. Rotational invariance allows us to consider only the z-x plane, for instance. If $\tan\alpha=z/x$ defines the slope of lines passing through a given point and the origin, it is straightforward to show that, in the long-distance regime and to leading order,

$$\frac{\rho_z}{\rho_x}\sim\tan\alpha-\frac{A}{x},\quad A=\delta\left(\frac{1-e^{-2\zeta\delta\sin\alpha}}{1+e^{-2\zeta\delta\sin\alpha}}\right). \tag{7}$$

The above equation may be approximately integrated by supposing A to be a constant coefficient. To leading order, asymptotic gradient lines are straight lines that point towards an α-dependent center situated at $(0,A)$, on the internuclear axes and between both nuclei. Simple simulations corroborate our findings. Figure 8 shows a model gradient vector field for a hypothetical H_2 molecule described by a basis set composed of two s primitives with $\zeta_1=7.0$ a.u. and $\zeta_2=0.01$ a.u.

The figure also shows that the space is divided into regions of dominance associated with each primitive. These regions are depicted as dashed circles. It is seen that within these regions the gradient lines tend to be linear, with notorious slope jumps on crossing a transition region, and that the full phenomenon reminds a refraction event in optics. This analogy is not casual, since one can parallel equidensity surfaces with constant action surfaces in the discussion of propagation of light through media with variable index of refraction.

In a general molecule and assuming that the asymptotic density may be expressed as an exponentially decreasing function of a suitably defined distance to the molecular frame times a bounded angular coefficient, $\rho\sim e^{-\eta r}g(\theta,\phi)$, it is also easy to show that equations similar to Eq. (7) hold for ρ_z/ρ_x, ρ_z/ρ_y, and ρ_y/ρ_x, this time with bounded $A(\theta,\phi)$ coefficients dependent on the molecular structure. At large distances from the molecular center, the gradient field thus seems to radiate towards the molecule.

In summary, the inaccessibility of integrated Gaussian curvatures from unbounded surfaces is, therefore, a general problem due to the computational approximations used to solve the Scrödinger equation.

IV. LOCAL CURVATURE OF INTERATOMIC SURFACES AT BOND CRITICAL POINTS

In the last section, we have presented a number of results regarding the total curvatures of interatomic surfaces. We have found that (i) the calculation of C^F is subjected to severe computational problems and (ii) the shape of the IAS near a bcp is fairly transferable among different computational conditions in a region surrounding the bcp that is, unfortunately, not well defined. A solution for this situation has already been advanced and consists of examining the local value of the curvature at the critical point. This is a parameter that is expected to satisfy transferability among systems as well as sensitivity to different chemical environments. It also shares the spirit of the AIM theory in being a single scalar obtained at the chemically important critical points.

A. Analytical curvatures at bcp's

First, it is useful to remember that our flux lines are the solutions of a gradient dynamical system. This means that the geometry of these curves is well at hand. In this section we will suppose Cartesian reference systems. The position vector of gradient lines will be labeled as $\boldsymbol{r}$ and their coordinates x,y,z or x_α, $\alpha=1,2,3$. If we choose a conventional t parametrization, the chain rule allows us to write all the derivatives with respect to the parameter in terms of successive derivatives of ρ. For instance,

$$\begin{aligned}&\dot{x}_\alpha=\rho_\alpha,\\ &\ddot{x}_\alpha=\rho_{\alpha\beta}\rho_\beta,\\ &\dddot{x}_\alpha=\rho_{\alpha\beta\gamma}\rho_\beta\rho_\gamma+\rho_{\alpha\beta}\rho_{\beta\gamma}\rho_\gamma,\\ &\ldots,\end{aligned} \tag{8}$$

where we have used the Einstein summation convention. In this way the Frenet frame can be obtained at each point of the curve. The unit tangent $\boldsymbol{t}$ is the unit vector in the direction of the gradient, $\boldsymbol{t}=\dot{\boldsymbol{r}}/|\dot{\boldsymbol{r}}|$, and

$$\kappa \boldsymbol{n}=\frac{d^2\boldsymbol{r}}{ds^2}=\frac{\ddot{\boldsymbol{r}}|\dot{\boldsymbol{r}}|^2-\dot{\boldsymbol{r}}(\dot{\boldsymbol{r}}\cdot\ddot{\boldsymbol{r}})}{|\dot{\boldsymbol{r}}|^4}, \tag{9}$$

and $\boldsymbol{b}=\boldsymbol{t}\times\boldsymbol{n}$. The curvature or torsion of gradient lines may then be computed easily at any nonsingular point. Critical points are to be handled by special techniques, as those developed below.

As IASs are regarded, it is convenient to choose as reference frame the one constructed with the unit eigenvectors of the Hessian of the density at the bcp and center it also at the critical point. The eigenvector corresponding to the positive Hessian eigenvalue will define our z axis, and the principal vectors with negative eigenvalues will be chosen as x,y directions so as to have a right-handed frame.

As a first approximation to the structure of the flow around the bcp, one integrates the linearized dynamical system, $\dot{x}_\alpha=\rho^0_{\alpha\alpha}x_\alpha$, where the zero superindex indicates derivatives obtained at the critical point, to obtain $x_\alpha=x_\alpha(0)\exp(\rho^0_{\alpha\alpha}t)$, which can be explicitly solved for any pair of coordinates, $x_\alpha/x_\alpha(0)=[x_\beta/x_\beta(0)]^{(\rho^0_{\alpha\alpha}/\rho^0_{\beta\beta})}$, $\alpha\neq\beta$. This teaches us that, except in the degenerate case $\rho^0_{xx}=\rho^0_{yy}$, the projection onto the x-y plane of almost all the gradient lines that form the IAS approach the bcp with either zero or infinite slope, depending on which of the ρ^0_{yy},ρ^0_{xx} eigenvalues is larger, and that in the surroundings of the bcp the lines crowd heavily around one of either the y or x axes.

In the full nonlinear system, the flux lines will display large torsions on elevating in the z direction, not being of much use to obtain the curvature of the surface at the bcp. The naive vision of an IAS as being traversed by a homogeneous set of gradient lines is, simply, not true. Two particular orthogonal lines do not bend—i.e., do not display curvature in the x-y plane—in the linearized system. These are the pairs of gradient lines along the eigenvectors, $y(0)=0$, or $x(0)=0$.

We are going to obtain an analytical expression for the osculating paraboloid introduced in Sec. II at a bcp and directly read the Gaussian curvature of the IAS at the critical point. Then we will also obtain the principal normal and the curvature of a flux line along an eigenvector of $\rho_{\alpha\beta}$ at a critical point and show how the latter are related to the former.

Let us consider the following expression for the osculating paraboloid in the previously defined coordinates,

$$z=\frac{1}{2}ax^2+\frac{1}{2}by^2+cxy+\mathcal{O}(|x|^3), \tag{10}$$

and use a Taylor expansion of the nonlinear dynamical system around the bcp:

$$\dot{x}_\alpha=\rho^0_{\alpha\alpha}x_\alpha+\frac{1}{2}\sum_{\beta,\gamma}\rho^0_{\alpha\beta\gamma}x_\beta x_\gamma+\mathcal{O}(|x|^3). \tag{11}$$

If we explicitly particularize the last equation for z and substitute Eq. (10) in it, keeping terms up to second order in the coordinates, we get

$$\dot{z}=\frac{1}{2}(a\rho^0_{zz}+\rho^0_{xxz})x^2+\frac{1}{2}(b\rho^0_{zz}+\rho^0_{yyz})y^2+c(\rho^0_{zz}+\rho^0_{xyz})xy+\mathcal{O}(|x^3|). \tag{12}$$

This equation can be compared with that obtained when we directly take the parameter derivative of Eq. (10), substitute the right-hand side derivatives by their corresponding expansions in Eq. (11), and keep terms only up to second order:

$$\dot{z}=a\rho^0_{xx}x^2+b\rho^0_{yy}y^2+c(\rho^0_{xx}+\rho^0_{yy})xy+\mathcal{O}(|x^3|). \tag{13}$$

Identifying terms, we finally obtain

$$a=\frac{\rho^0_{xxz}}{2\rho^0_{xx}-\rho^0_{zz}},$$

$$b=\frac{\rho^0_{yyz}}{2\rho^0_{yy}-\rho^0_{zz}},$$

$$c=\frac{\rho^0_{xyz}}{\rho^0_{xx}+\rho^0_{yy}-\rho^0_{zz}}. \tag{14}$$

These a and b are then the normal curvatures of the paraboloid along the x and y directions. The principal curvatures κ_1, κ_2 together with the principal directions of curvature are easily found by diagonalizing the

$$\mathcal{H}=\begin{pmatrix} a & c \\ c & b \end{pmatrix} \tag{15}$$

bilinear form. The Gaussian (K) and mean (H) curvatures may be directly obtained from it:

$$K=\det(\mathcal{H})=ab-c^2,$$

$$H=\mathrm{tr}(\mathcal{H})=a+b. \tag{16}$$

It is interesting to notice that when ρ^0_{xyz} is not zero the principal directions of curvature do not coincide with the principal directions of the Hessian of ρ. This means that the osculating paraboloid at the bcp is rotated with respect to the frame chosen—namely, the eigendirections of the electron density Hessian at the bcp.

We can also use Eq. (9) to obtain the $d^2\boldsymbol{r}/ds^2$ vector for gradient lines at critical points. A simple strategy consists of substituting the Taylor expansion of Eq. (11) into Eq. (9) and

extract its limit at the bcp. We are particularly interested in the curvatures along the principal directions of the Hessian—namely, the $\boldsymbol{i}$, $\boldsymbol{j}$ directions in the principal reference frame. Let us consider, for instance, the z component of the $\kappa\boldsymbol{n}$ vector of the gradient lines starting or ending along the $\boldsymbol{i}$ direction:

$$\kappa \boldsymbol{n}_z = \frac{\ddot{z}(\dot{x}^2+\dot{y}^2)-\dot{z}(\dot{x}\ddot{x}+\dot{y}\ddot{y})}{(\dot{x}^2+\dot{y}^2+\dot{z}^2)^2}. \tag{17}$$

As the linearized system shows us, its projection onto the x-y or x-z plane does not contain linear terms in x, so $z \sim \alpha x^2$ and $y \sim \beta x^2$, to leading order. The denominator of the previous equation is, then, $(\rho^0_{xx})^4 x^4 + \mathcal{O}(|x^6|)$. By expanding the numerator in a similar way and keeping only leading order terms, we can conclude easily that $(\kappa\boldsymbol{n})_z = a$, where a is that defined in Eq. (14). This conclusion could have been previously advanced, for the normal curvature of all the curves contained in a given surface that are tangent at a point are equal, as stated in Sec. II. Applying repeatedly this argument, we arrive at the following expression:

$$\kappa \boldsymbol{n} = \frac{\rho^0_{xxy}}{2\rho^0_{xx}-\rho^0_{yy}}\boldsymbol{j} + \frac{\rho^0_{xxz}}{2\rho^0_{xx}-\rho^0_{zz}}\boldsymbol{k}, \tag{18}$$

which defines the principal normal and curvature of the gradient lines corresponding to the Hessian eigenvector along x. A permutation of indices takes us to analogous expressions for the normals and curvatures along the other two eigendirections. Here it is also worth noticing that the principal normal to a gradient line along, say, the x direction may not be parallel to the surface normal vector.

B. Implementation details

The expressions derived so far have been coded into our PROMOLDEN (Ref. 24) code. Some care has to be taken in the coordinate transformation that takes us to the principal frame used in the previous expressions. If $u_{\alpha\beta}$ is the matrix that diagonalizes the Hessian at the critical point—that is, the rotation matrix that moves the molecular frame into the principal frame at the bcp—then the third-rank tensor of the third derivatives of ρ may be transformed from the molecular frame in which it is calculated into the principal frame by making profit of the tensor condition

$$\rho_{\alpha'\beta'\gamma'} = \rho_{\lambda\mu\nu} u_{\lambda\alpha} u_{\mu\beta} u_{\nu\gamma}, \tag{19}$$

where the Einstein convention has been used and the primed derivatives are those calculated in the principal frame.

These results are by no means restricted to bcp's and may be applied to flux lines along eigenvectors of the density Hessian at general critical points. When used for the bond path direction at the bcp, we obtain the curvature of the bond path line. This is known to be a very interesting magnitude,[1] for some bond paths display rather large curvatures that have been related to chemical concepts like molecular strain, bonding instabilities, etc. Sometimes, the curvatures of bond paths are very small, but not zero. These are situations rather difficult to detect by either inspection or numerical calculation, which our analytical approach may unveil.

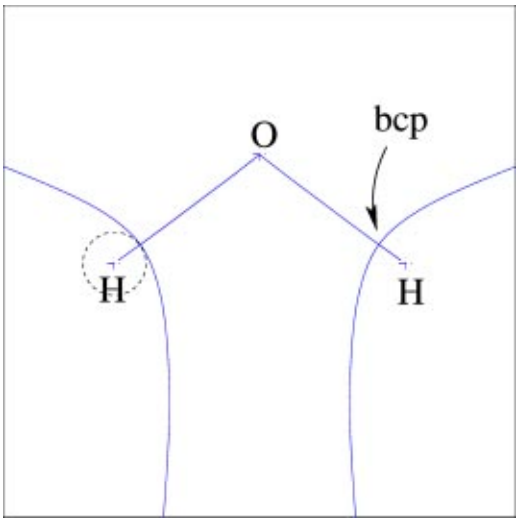

FIG. 9. Bond paths and IASs projected on the molecular plane of a HF/TZV++$(2p,3d1f)$ H_2O molecule. $R(\mathrm{O-H}) = 1.777$ bohr, $\widehat{\mathrm{HOH}} = 106.46°$. See the text for details.

Our implementation of the analytical derivatives code is, otherwise, straightforward. All the local magnitudes defined in this work are now routinely computed at every bcp that our algorithms find and have become a standard part of the information that is collected at each critical point.

Let us conclude this section with a concrete example. Figure 9 shows the bond paths and projection of the IASs on the molecular plane in a HF/TZV++$(2p,3d1f)$ water molecule. The curvature parameters of the IASs at the two equivalent bcp's are $\kappa_1 = 1.2206$ bohr^{-1} and $\kappa_2 = 1.2644$ bohr^{-1}, with the principal curvature directions coinciding with the Hessian eigenvectors, $K = 1.5433$ bohr^{-2} and $H = 1.2425$ bohr^{-2}. The O–H IAS is a rather curved, almost parabolic surface near the bcp, actually slightly more curved in the direction orthogonal to the molecular plane than in that contained in it. However, if we consider that the distance from the bcp to the H atom is 0.2601 bohr, we realize that the radius of curvature as seen in the picture, $r = \kappa_1^{-1} = 0.8193$ bohr, is 3 times as large. The surface, as seen from the hydrogen, is far from a a patch of a sphere centered at its nucleus.

The bond path at the bcp is, surprisingly, not a straight line, but curves slightly, with $\kappa = 0.0579$ bohr^{-1}, towards the other bond. This, as previously advanced, is hardly noticeable to the naked eye. It can be interpreted as a remnant of the bifurcation catastrophe ocurring when an oxygen atom attacks a H_2 molecule and the H—H bond path splits into two very curved equivalent O—H bonds.[25]

V. CONCLUSIONS

In this work we have investigated the geometry of interatomic surfaces, paying special attention to their curvature at the bond critical point. Previous studies[15] had focused on the numerical calculation of the integral (total) Gaussian curvature of such surfaces and had unveiled several interesting correlations between the total curvatures and chemically interesting concepts.

We have shown that the global Gauss–Bonnet theorem introduces stringent constraints on the possible values that the total Gaussian curvatures may attain. On the one hand, C^F is a theoretically sound property but, on the other, it is practically inaccessible. In unbounded IASs, like those found in many small, isolated molecules, its value is controlled by the asymptotic behavior of gradient lines at infinity. As explicitly discussed, in the revolution IASs of diatomics C^F is determined by the slope of the generating curve with respect to the osculating plane. Moreover, the analysis of the behavior of gradient lines at large distances from the molecular frame shows that K is determined by the characteristics of the basis sets used in the calculation—in particular, by the outermost primitive in the basis. We have demonstrated how all of the gradient lines seem to radiate from the center at which the most diffuse function is located. This means that very small changes in the basis set may induce enormous changes in the total curvatures. As a result, we may safely say that global curvatures of unbounded IASs are not computable. In completely bounded surfaces the global curvatures can be obtained, but will not be transferable to unbounded cases.

The problems posed by these constraints have guided us to propose the local curvature of IASs at bcp's as a geometrical measure in IASs. We have shown how the consideration of the gradient dynamical system generated by the electron density allows us to obtain analytical formulas for the curvatures of gradient lines at critical points and used them to present analytical expressions for the Gaussian curvature of IASs at bcp's. These expressions involve only second and third derivatives of the density at the critical point and are particularly easy to code. One can thus obtain K at almost no extra cost when analyzing the topology of a molecular system.

ACKNOWLEDGMENT

This work has been partially supported by the Spanish Ministerio de Ciencia y Tecnología, Project No. BQU2000-0466.

[1] R. F. W. Bader, *Atoms in Molecules* (Oxford University Press, Oxford, 1990).
[2] R. F. W. Bader and H. Essén, J. Chem. Phys. **80**, 1943 (1984).
[3] T. S. Koritsanszky and P. Coppens, Chem. Rev. **101**, 1583 (2001).
[4] R. F. W. Bader, T. T. Nguyen-Dang, and Y. Tal, Rep. Prog. Phys. **44**, 893 (1981).
[5] A. Martín Pendás, A. Costales, and V. Luaña, Phys. Rev. B **55**, 4275 (1997).
[6] F. Biegler-König, T. T. Nguyen-Dang, Y. Tal, R. F. W. Bader, and A. J. Duke, J. Phys. B **14**, 2739 (1981).
[7] A. Martín Pendás, J. Chem. Phys. **117**, 965 (2002).
[8] P. L. A. Popelier, Theor. Chem. Acc. **105**, 393 (2001).
[9] J. Cioslowski and B. B. Stefanov, Mol. Phys. **84**, 707 (1995).
[10] J. Cioslowski and B. B. Stefanov, J. Chem. Phys. **105**, 8741 (1996).
[11] P. L. A. Popelier, Theor. Chim. Acta **87**, 465 (1994).
[12] P. L. A. Popelier, Comput. Phys. Commun. **93**, 212 (1996).
[13] V. Luaña, A. Costales, and A. Martín Pendás, Phys. Rev. B **55**, 4285 (1997).
[14] A. Martín Pendás, A. Costales, and V. Luaña, J. Phys. Chem. B **102**, 6937 (1998).
[15] P. L. A. Popelier, Can. J. Chem. **74**, 829 (1996).
[16] M. P. do Carmo, *Differential Geometry of Curves and Surfaces* (Prentice-Hall, Englewood Cliff, NJ, 1976).
[17] R. D. Kamien, Rev. Mod. Phys. **74**, 953 (2002).
[18] H. Iseri, *Smarandache Manifolds* (American Research Press, NM, 2002).
[19] P. Mori-Sánchez, Ph.D. thesis, University of Oviedo, 2002.
[20] V. Luaña, A. Martín Pendás, J. M. Recio, E. Francisco, and M. Bermejo, Comput. Phys. Commun. **77**, 107 (1993).
[21] M. Hoffmann-Ostenhoff and T. Hoffmann-Ostenhoff, Phys. Rev. A **16**, 1782 (1977).
[22] P. N. Brown, G. D. Byrne, and A. C. Hindmarsh, J. Sci. Stat. Comput. **10**, 1038 (1989).
[23] M. W. Schmidt, K. K. Baldridge, J. A. Boatz, *et al.* J. Comput. Chem. **14**, 1347 (1993).
[24] A. Martín Pendás, computer code PROMOLDEN (unpublished), available from the author upon request.
[25] R. F. W. Bader, T. T. Nguyen-Dang, and Y. Tal, Rep. Prog. Phys. **44**, 893 (1981).